

3D-vortex labyrinths in the near field of solid-state microchip laser.

A.Yu.Okulov*

*P.N.Lebedev Physical Institute of Russian Academy of Sciences
Leninsky prospect 53, 119991 Moscow, Russia*

(Dated: February 12, 2007)

The spatiotemporal vortex lattices generated in high Fresnel number solid-state microchip lasers are studied in connection with Talbot phenomenon generic to spatially periodic electromagnetic fields. The spatial layout of light field is obtained via dynamical model based on Maxwell-Bloch equations for class-B laser, discrete Fox-Lee map with relaxation of inversion and static model based on superposition of copropagating Gaussian beams. The spatial patterns observed experimentally and obtained numerically are interpreted as nonlinear superposition of vortices with helicoidal phase dislocations. The usage of vortex labyrinths and Talbot lattices as optical dipole traps for neutral atoms is considered for the wavelength of trapping radiation in the range $0.98 \div 2.79 \mu m$. The separable optical trapping potential is mounted as a sum of array of vortex lines and additional parabolic subtrap. The factorization of macroscopic wavefunction have led to analytical solution of Gross-Pitaevski equation for ground state of ensemble of quantum particles trapped in vortex labyrinth and in spatially - periodic array of Gaussian beams.

PACS numbers: 03.75.Lm., 42.50.Vk., 42.60.Jf, 42.65.Sf., 47.32.Cc

I. INTRODUCTION

Optical dipole traps for neutral atoms [1] are a subject of considerable interest. Recent years there appeared a certain amount of proposals of increasing complexity of trapping EM-field. Apart from a relatively simple geometrical patterns like standing plane-wave patterns[2], evanescent wave mirrors[3], toroidal traps which utilize the intensity distribution of Gaussian-Laguerre (GL) beams in beam bottleneck [4] a several proposals were made which utilize the arrays of Gaussian beams, both phase-locked [5, 6] and unlocked ones [7]. The interference inherent to phase-locking provides interesting configurations of intensity distribution, phase gradients and electromagnetic (EM) momentum density [8, 9]. The multiply connected EM-momentum distribution is the cause of the angular momentum transfer to macroscopic bodies (e.g. dielectric ball) [10] or to trapped BEC with possibility of generating vortex matter waves of different geometries by external optical means.

The EM-field configuration under consideration is based upon properties of self-imaging optical fields[11, 12]. The difference between phase-locked array of zero order Gaussian beams and experimentally obtained phase-locked array of optical vortices (OV) in the near field of solid-state microchip laser [13] is that the latter consists of array of parallel vortex lines with opposite circulations and topological charges ℓ_{EM} (TC) (fig. 1) [5]. In contrast to earlier proposals where individual loading and addressing of trapping sites was implied [7] this OV array have sophisticated configuration of intensity [5] and EM-momentum density of trapping field. Due to this configuration the BEC suspended in trapping EM-field might have macroscopic wavefunction of complex form composed of array of superfluid vortices (SFV). The mechanism of SFV formation will be considered based upon light-induced torque experienced by isolated resonant atom interacting with Gaussian-Laguerre beam having phase singularity. It was show by Allen et al.[8] the value of torque in saturation limit is proportional to TC: $T = \hbar \ell_{EM} \Gamma$. The origin of T is due to nonzero azimuthal EM-momentum component. The azimuthal Doppler shift corresponding to such motion had been onrserved[9]. This torque might have an appreciable value even in nonresonant case, although it is significantly reduced by the multiple of Δ/Γ , where Δ - is detuning, Γ - is linewidth[8]. As a result an azimuthal component of EM-momentum is transferred to atom in such a way that it will move around phase singularity - the direction of rotation is fixed by TC of trapping beam. This is the cause of circular motion of BEC trapped in such isolated toroidal trap.

The goal of current communication is to present the maximally transparent and simple analytical solution in order to track transfer of angular momentum from optical vortex array (OVA) to trapped BEC. The configuration of intensity and phase of EM-field of OVA has rather complicated, multinode structure. In order to get analytic solution for ground state macroscopic wavefunction Ψ trapped by such array, the special optical pancake-like potential (fig. 1) will be constructed which allows the separation of variables in Gross-Pitaevsky equation[2]. Next the procedure

*Electronic address: okulov@sci.lebedev.ru; URL: <http://sites.lebedev.ru/okulov>

applied previously to elongated *sech*²- profile optical trap [14] will be used. Due to special adjustment of potential it is possible to extract an analytic factorized solution for Ψ in the form of superposition of elementary equispaced vortices. The solution supports the proposal that small but unavoidable EM-torque existing in OV even at large detuning from resonance Δ impose the correlation between TC of BEC vortices and TC of the elements of OVA. Owing to correlation the ground state Ψ carries the net angular momentum close to zero, while local angular momentum distribution is formed via periodic lattice of SFV with alternating topological charges. There is a remarkable contrast with superfluid in "rotating bucket" trap: while angular momenta of SFV in bucket are co-directed [15, 16] the BEC vortices trapped by OVA are counter-directed from site to site.

Thus in the net sum of angular momenta each SFV of positive topological charge is compensated by the SFV with negative charge and total angular momentum tends to zero. Meantime the mutual subtraction of angular momenta (vectorial) of adjacent vortices in the net sum does not mean the mutual subtraction of rotational energies, which are the positive scalars. The ground state carry substantial amount of rotational kinetic energy of condensate containing N particles of mass m per unit volume, namely $E_{rot} = N_{vortices} N \pi \hbar^2 \ln(b/a) \chi / m$, b -diameter of vortex core, a -interatomic distance, χ - length of vortex [16]. This feature of macroscopic wavefunction Ψ trapped by vortex array might be useful from the point view of diminishing the decoherence induced by environment and topological quantum computing [17].

II. SQUARE VORTEX LATTICES

Recent advances in controlling the geometry of solid-state microchip lasers [13] offer the possibility of reliable control of spatiotemporal optical patterns. Compared to semiconductor lasers the host medium composed of dielectric crystal doped by neodymium Nd^{+3} or other rare earth ions (Er^{+3} , Tm^{+3} , Ho^{+3} , Yb^{+3}) offers a possibility of rather accurate manipulation of emission patterns. The changes of the geometry and crystallographical properties of host crystals, curvature and reflectivity of output couplers, spatial distribution of optical pumping give the rich variety of spatial patterns. Among them the square vortex lattices (SVL) observed in quasi plane parallel cavity [13] are of fundamental interest. These lattices demonstrate impressive spatial coherence: the relaxation oscillations of class-B high Fresnel number solid-state microchip laser [13] with Fresnel number in the range $N_f \approx 100 \div 1000$ are characterized by single peak at frequency about $(\sqrt{T_1 \tau_c})^{-1}$. This is the firm evidence of single-longitudinal and single transverse mode behaviour. The theoretical analysis was based on Swift-Hohenberg equation, resulted from standard set of Maxwell-Bloch equations, when finite gain linewidth T_2^{-1} is taken into account [18]:

$$\begin{aligned} \frac{\partial E(\vec{r}, t)}{\partial t} + \frac{E(\vec{r}, t)}{(\tau_c + T_2)} + \frac{i \tau_c c}{2k(\tau_c + T_2)} \Delta_{\perp} E(\vec{r}, t) + \\ \frac{T_2^2}{\tau_c(\tau_c + T_2)^2} \left(\frac{\tau_c c}{k} \Delta_{\perp} + \delta\omega T_2 \right)^2 E(\vec{r}, t) = \frac{\sigma c N_0 L_a E(\vec{r}, t) (1 + i\delta\omega T_2)}{2L_r (1 + \sigma T_1 c \epsilon_0 |E|^2 / \hbar\omega)} \end{aligned} \quad (1)$$

where τ_c - is photon lifetime in cavity, $k=2\pi/\lambda$ - wavenumber, σ - stimulated emission crosssection, $\delta\omega$ - detuning of lasing frequency from center of gain line, N_0 - density of inverted resonant atoms per unit volume, T_1 - inversion lifetime (longitudinal relaxation lifetime), L_a - thickness of active medium, L_r - length of resonator, c - speed of light, ϵ_0 - dielectric constant, $\Delta_{\perp} = \nabla_{\perp}^2$ [18, 20].

The alternative model with discrete time step equal to $\tau_c = 2L_r/c$ (time of bouncing of radiation between mirrors) which utilize standard rate equations of class-B laser written at n -th step for electric field [5, 19]:

$$E_{n+1}(\vec{r}) = f(E_n(\vec{r})) = \frac{\sigma L_a N_n(\vec{r}) E_n(\vec{r}) (1 + i\delta\omega T_2)}{2} + E_n(\vec{r}), \quad (2)$$

inversion:

$$N_{n+1}(\vec{r}) = N_n(\vec{r}) + \left[\frac{N_0(\vec{r}) - N_n(\vec{r})}{T_1} - \sigma N_n(\vec{r}) c \epsilon_0 |E|^2 / \hbar\omega \right] \frac{2L_r}{c}, \quad (3)$$

and nonlocal integral mapping evaluating the field via fast Fourier transform at each timestep:

$$E_{n+1}(\vec{r}) = \int_{-\infty}^{\infty} \int_{-\infty}^{\infty} K(\vec{r} - \vec{r}') f(E_n(\vec{r}')) d^2 \vec{r}', \quad (4)$$

where the kernel K for the nearly plane-parallel Fabry-Perot cavity of microchip laser with transverse localization via aperture $D(\vec{r}')$ has the form [11]:

$$K(\vec{r} - \vec{r}') = \frac{ikD(\vec{r}')}{2\pi L_r} \exp [ik(\vec{r} - \vec{r}')^2 / 2L_r], \quad (5)$$

gives the similar spatiotemporal picture of transverse modes for 2-D transverse dimensions case. The following parameters were chosen: $T_1 = 2 \cdot 10^{-4} \text{ sec}$, $L_r = 1 \text{ mm}$, for Nd^{+3} -doped crystals $\sigma = (1.2 - 0.6) \cdot 10^{-20} \text{ cm}^2$, $N_0 = 10^{16} \text{ cm}^{-3}$, $\delta\omega T_2 = -0.1$,

Near lasing threshold the mode has a distribution of intensity of rectangular grating of bright and dark spots : the latter are vortex cores. The nonlocal integral mapping proved to be successful in computation the near field distribution as well. Quite unexpectedly in most runs the parallel vortex lines were obtained (fig. 1) [5] rather than periodic array of bright and dark spots, typical to Talbot phenomenon[11]. The origin of parallel vortex lines is interpreted as nonlinear superposition of vortices with helicoidal phase dislocations. Next sections are devoted to the possible linear equivalent of nonlinear optical vortex lattices.

III. TALBOT LATTICES

Consider the phase-locked rectangular lattice of zero-order Gaussian beams located at sites $\vec{r}_{jx,jy}$ [11] separated by period p , jx, jy - are discrete indices corresponding x and y coordinate of a given site. For simplicity let us assume that polarization is linear, thus spin of light is zero. At $z = 0$ plane the electric field E is given by expression:

$$E(\vec{r}, 0) = E_0 \sum_{jx,jy} \exp[-|\vec{r} - \vec{r}_{jx,jy}|^2 / (2d^2)] \quad (6)$$

After paraxial propagation of distance z the electric field $E(\vec{r}, z)$ is transformed into:

$$E(\vec{r}, z) = E_0 \frac{i \exp[ikz]}{(1 - iz/kd^2)} \sum_{jx,jy} \exp\left[-\frac{|\vec{r} - \vec{r}_{jx,jy}|^2}{2d^2(1 - iz/(kd^2))}\right] \quad (7)$$

The constructive interference between adjacent beams produces periodic interference patterns in different z -planes. The initial periodical pattern is reproduced at so-called Talbot-distances $z_t = 2p^2/\lambda$. In the intermediate planes $z_t/4m$ the coarser lattices with periods p/m are produced[21, 22]. As a result a 3D lattice of bright spots is formed (fig. 2).

Each spot could serve as potential well for neutral atoms [1, 2, 5, 6], because intensity gradient will attract or repulse the atomic dipoles depending the sign of detuning of radiation frequency from resonance. At low frequencies (red-detuning) atomic dipole oscillates in-phase with trapping field and tries to align parallel to electric field. Thus potential energy of dipole $U = -d E(\vec{r})$ is lower in local maxima of intensity and atoms are collected at bright spots. On the other hand at frequencies above the resonance (blue-detuning) atomic dipole oscillates out-of-phase and they have tendency to align anti-parallel to electric field. In this blue-detuned case potential energy of dipole is higher in local maxima of intensity and atoms are repelled into dark regions.

This geometry of trapping in integer and fractional Talbot planes based on superposition of co-propagating [5] zero-order Gaussian beams was considered including possibility of manipulation of optical lattice geometry via mutual polarization [6] of beams.

IV. ARTIFICIAL VORTEX LABYRINTH

Consider now the periodic array of Gaussian-Laguerre vortex beams with helicoidal phase dislocations (fig. 3):

$$E(\vec{r}, z = 0) \approx E_0 \sum_{jx,jy} (|\vec{r} - \vec{r}_{jx,jy}|) \exp(-|\vec{r} - \vec{r}_{jx,jy}|^2 / d^2) \exp(-|\vec{r}|^2 / D^2) \exp[i \ell_{EM} \text{Arg}(\vec{r} - \vec{r}_{jx,jy}) + i \pi(jx + jy)]. \quad (8)$$

The topological charge ℓ_{EM} is assumed to be unity, the neighbouring beams (components of the sum (8)) are π -shifted. The apodization function $\exp(-|\vec{r}|^2 / D^2)$ is added in order to suppress the maximum of interference pattern at the edge of array. The beams centers are placed in the centers of rectangular grid $\vec{r}_{i,j}$ of period p whose axes are parallel to X, Y . The overlapping beams produce interference pattern formed by two arrays of bright and dark spots rotated at 45° angle with respect to initial array of GL beams. The dark spots are of two kinds: one lattice of spots coincides with lattice of initial vortices(8), the other one is produced by interference and it is shifted at distance $p/\sqrt{2}$ along diagonal of initial lattice. The resulting interferogram has apparent 45° tilt compared to lattice of initial vortices (fig. 3).

The topological charges of dark spots (vortices) flip from one site to another. The interesting feature of this interference pattern is the distribution of angular momentum [12]. The initial array of GL beams carries unit circulation and corresponding angular momentum at each site. The interferogram (fig. 4) contains additional array of vortices with alternative charges. The net angular momentum tends to be close to zero, because at the central part of array each positively directed TC ℓ_{EM} is compensated by the four adjacent negative ones having charge $-\ell_{EM}$. The elementary cell of such a lattice consists of two π -shifted initial vortices with co-directed charges ℓ_{EM} located at diagonal and two counter-directed charges $-\ell_{EM}$ (π -shifted too) placed at the other diagonal of cell. The period p of initial pattern was taken being equal to $30\mu m$ while width of each initial beam was set $w_{GL} = 22\mu m$ in order to provide significant mutual overlapping of vortices.

The longitudinal distribution of intensity of optical vortex array is composed of periodic (with period p) hollow tubes - vortex cores. Apart from Talbot gratings which are reproduced by diffraction at $z_t = 2p^2/\lambda$ planes with corresponding period division in between the vortex array under consideration keeps its shape within Rayleigh range, i.e. at distances $z < D^2/\lambda$. The form of channels is kept by interference of adjacent vortices, whose helical wavefronts are perfectly matched in elementary cell (fig. 4).

Consider now the interaction of individual atoms with single optical beam carrying topological charge. The gradient force will attract the "red" detuned atomic dipole to the intensity maximum of an isolated first order Gaussian-Laguerre beam - "doughnut" beam (fig. 5), i.e. to ring around phase singularity. As a result the cloud of cold atoms will be accumulated near the maximum of intensity or "doughnut" as follows from variational solution of Gross-Pitaevsky equation (GPE) [2]:

$$i\hbar \frac{\partial \Psi(\vec{r}, t)}{\partial t} = -\frac{\hbar^2}{2m} \Delta \Psi(\vec{r}, t) + V_{ext}(\vec{r}) \Psi(\vec{r}, t) + \frac{4\pi\hbar^2 a}{m} \Psi(\vec{r}, t) |\Psi(\vec{r}, t)|^2, \quad (9)$$

with trapping potential V_{ext} of the form

$$V_{ext}(\vec{r}) = \frac{m\omega_z^2 z^2}{2} - \alpha(\omega) \epsilon_0 |E_0|^2 [r^2 \exp(-r^2/(2w_{GL}^2))] \quad (10)$$

$\alpha(\omega)$ - polarizability of atom[1], m - mass of particle, a - scattering length.

This approximate variational solution for GPE groundstate macroscopic wavefunction has the form of Gaussian-Laguerre function [24]:

$$\Psi(\vec{r}, t) = |\vec{r}| \exp(-|\vec{r}|^2/(2w_r^2) - z^2/(2w_z^2) + i\ell_{BEC} \phi), \quad (11)$$

where ℓ_{BEC} is the topological charge of this vortex Ψ solution. Hence the probability distribution of finding atom $|\Psi(\vec{r}, t)|^2$ is similar to the intensity distribution of trapping field as pointed out in [24]. More information could be obtained from the study of phase structure of wavefunction and comparison of topological charges of trapping EM-beam and BEC vortex. Using Madelung transform

$$\Psi(\vec{r}, t) = \sqrt{\rho(|\vec{r}|, \phi, t)} \exp(i\theta(|\vec{r}|, \phi, t)) \quad (12)$$

it is easy to realize that there exists flow of "probability fluid" with velocity \vec{v} proportional (parallel) to the phase gradient lines:

$$v(\vec{r}, t) = \frac{\hbar}{m} \nabla \theta(\vec{r}, t) \quad (13)$$

Such "flow of wavefunction" occurs around the z -axis (beam axis). The "flow" described by (11) is potential and conservative as it should be for superfluid. This picture is complicated by vorticity of EM-momentum, inherent to GL-beams [9]. Strictly speaking the rotation of classical dipole around core is accelerated by nonconservative torque induced by azimuthal force circulating around vortex core. For two-level atom the value of torque T is given by [8]:

$$T = \hbar \ell_{EM} \Gamma \left[\frac{1}{1 + I + \Delta^2/\Gamma^2} \right] \quad (14)$$

In saturation limit T is simply: $T = \hbar \ell_{EM} \Gamma$. In nonresonant case this torque reduces as Δ^{-2} (detuning of trapping field from resonant frequency of dipole) but it affects both classical and quantum particles and both near and at large

detuning from the resonance. Consequently the loop integral of the azimuthal force over circular trajectory around core $\oint (\vec{F}_t \times \vec{r}) \cdot d\vec{l}$ is nonzero (fig. 5).

Due to this torque in classical picture the dipole (or small dielectric ball) placed in the doughnut beam will move "upwards" the helicoidal phase staircase, i.e. it will rotate around GL-beam axis. The direction of rotation is determined by topological charge ℓ_{EM} of the trapping beam (fig. 5). Qualitatively classical dipole is pushed by azimuthally periodic electric field - it happens because the phase of electric field oscillations at each point in circle around the center of beam is shifted with respect to neighbouring points. In the same way the small macroscopic object like glass ball placed at maximum of intensity of GL-beam will feel the "plane-wave-like" nonresonant pressure of light field. The associated azimuthal Doppler shift of the moving atom was observed recently experimentally[23]. Outside the resonance the origin of torque T is interpreted in similar way: the Poynting vector has component $S(\vec{r})_t$ tangent to helix and local flux of electromagnetic momentum push dipole along phase gradient, i.e. in azimuthal direction. The local density of EM-momentum $\vec{g} = \vec{S}/c^2$ is proportional to components of Poynting vector[9]:

$$\begin{aligned} S(\vec{r})_t &= \frac{\epsilon_0 \omega \ell_{EM} c^2}{r} |E(\vec{r})|^2 \\ S(\vec{r})_z &= \epsilon_0 c |E(\vec{r})|^2, \end{aligned} \quad (15)$$

where $S(\vec{r})_t$ - is tangential component of Poynting vector, $S(\vec{r})_z$ - is axial one, r - is the distance from optical vortex core, ω - is frequency of trapping field.

Analogously because of tangential component of EM-momentum the big dielectric ball with radius larger than GL-beam core and comparable to "doughnut" radius placed in center of GL-beam would rotate with acceleration because of the such torque and corresponding transfer of the angular momentum[10].

When loaded in optical vortex lattice (fig. 6) the atomic dipole will move around the adjacent vortex core with acceleration. The radius of rotation will increase until the dipole will approach the separatrix of the velocity fields. Next after certain amount of rotations around the vortex core it could jump to another vortex using bright spots between vortices as bridge (fig. 6). As mentioned earlier the speed of rotation is increased due to light-induced torque and radius of rotation is increased as well until dipole would come to another attractive center. The migration of dipole from one vortex to another is assisted by bright regions which serve as channels connecting vortices (fig. 3). This qualitative picture is complicated by azimuthally inhomogeneous distribution of intensity around each core.

Our aim now is to show that such classical motion have quantum mechanical counterpart resulting in the specific form of macroscopic wavefunction Ψ maintaining coherence all over array:

$$\begin{aligned} \Psi(\vec{r}) &\approx \sum_{jx, jy} (|\vec{r} - \vec{r}_{jx, jy}|) \exp(-|\vec{r} - \vec{r}_{jx, jy}|^2/d^2) \\ &\exp(-|\vec{r}|^2/D^2) \exp[i \ell_{BEC} \text{Arg}(\vec{r} - \vec{r}_{jx, jy}) + i \pi(jx + jy)]. \end{aligned} \quad (16)$$

Next section presents the method of solution of Gross-Pitaevsky equation with OV array trapping field $E(\vec{r})$ in the form (8).

V. SEPARABLE VORTEX ARRAY POTENTIAL FOR BEC

In order to get closed form solution for macroscopic Ψ it is worth to mention that azimuthal accelerating force has very small value, falling as Δ^{-2} under detuning from resonance[8]. Next let us introduce optical potential V_{ext} as a square modulus of trapping field $E(\vec{r}_\perp, z)$ [1]. The torque T will be taken into account as a "selection" rule for choosing distribution of topological charges ℓ_{BEC} in resulting solution.

It was shown recently [14] that Gross-Pitaevsky equation[2] in 3D-configuration:

$$\begin{aligned} i\hbar \frac{\partial \Psi(\vec{r}, t)}{\partial t} &= -\frac{\hbar^2}{2m} \Delta \Psi(\vec{r}, t) + V_{ext}(\vec{r}) \Psi(\vec{r}, t) + \\ &+ \frac{4\pi\hbar^2 a(\vec{B})}{m} \Psi(\vec{r}, t) |\Psi(\vec{r}, t)|^2, \end{aligned} \quad (17)$$

admits the application of standard method of separation of variables widely used for solution of partial differential equation, e.g. in quantum mechanics. The separation of variables means that wavefunction is factorized

$$\Psi(\vec{r}, t) = \Psi_\perp(\vec{r}_\perp, t) \Psi_\parallel(z, t) \quad (18)$$

and Hamiltonian is the sum of components each depending on a longitudinal variable z and a pair of transverse variables \vec{r}_\perp .

Following to [14] in order to separate variables and factorize the wavefunction let us choose trapping potential in the following form, as a sum of components depending on longitudinal coordinate z and transverse coordinates \vec{r}_\perp separately:

$$V_{ext}(\vec{r}_\perp, z) = V_z + V_\perp = \frac{m \omega_z^2 z^2}{2} - \alpha(\omega) \epsilon_0 |E(\vec{r}_\perp)|^2 + \frac{m \omega_\perp^2 (x^2 + y^2)}{2} \quad (19)$$

where $\alpha(\omega)$ is atomic polarizability[1] :

$$\alpha(\omega) = 6\pi\epsilon_0 c^3 \frac{\Gamma/\omega_0^2}{(\omega_0^2 - \omega^2 - i(\omega^3/\omega_0^2)\Gamma)} \quad (20)$$

trapping field $E(\vec{r}_\perp)$ is periodic function of transverse variables $\vec{r}_\perp = (x, y)$, composed of GL beams placed at the nodes (jx, jy) of rectangular grid of period p :

$$E(\vec{r}_\perp) \approx E_0 \sum_{jx, jy} \exp(-|\vec{r}_\perp|^2/D^2) (|\vec{r}_\perp - \vec{r}_{\perp, jx, jy}|) \exp[(\vec{r}_\perp - \vec{r}_{\perp, jx, jy})^2/d^2 + i\ell_{EM}\phi + i\pi(jx + jy)] \quad (21)$$

The additional parabolic well with frequency ω_\perp is introduced in (19) in order to get analytical solution. In order to avoid the interference between different trapping beams the usage of different carrier frequencies is recommended for longitudinal parabolic well $\frac{m \omega_z^2 z^2}{2}$, vortex array beam $E(\vec{r})$ and parabolic subtrap in (19). The characteristic scales of potential in longitudinal z direction and transverse direction are chosen to form "pancake trap" : $\omega_z \gg \omega_\perp$ (fig. 1). The opposite case of elongated trap with $\omega_z \ll \omega_\perp$ and "solitonic" longitudinal potential $V_z \approx \text{sech}^2(z)$ was considered earlier using analogous procedure [14].

The longitudinal part of wavefunction $\Psi_{||}(z, t)$ is obtained as a ground state of 1D harmonic oscillator:

$$i\hbar \frac{\partial \Psi_{||}}{\partial t} = -\frac{\hbar^2}{2m} \frac{\partial^2 \Psi_{||}}{\partial z^2} + \frac{m \omega_z^2 z^2}{2} \Psi_{||} \quad (22)$$

$$\Psi_{||} = (\frac{m\omega_z}{\pi\hbar})^{1/4} \exp[-m\omega_z z^2/(2\hbar) - i\omega_z t] \quad (23)$$

The transverse part of wavefunction $\Psi_\perp(\vec{r}_\perp, t)$ is to be obtained by solving "transverse" GPE:

$$i\hbar \frac{\partial \Psi_\perp}{\partial t} = -\frac{\hbar^2}{2m} \Delta_\perp \Psi_\perp + V_\perp(\vec{r}_\perp) \Psi_\perp + \frac{4\pi\hbar^2 a(\vec{B})}{m} \Psi_\perp |\Psi_\perp|^2 [\int_{-\infty}^{\infty} |\Psi_{||}(z, t)|^4 dz] / [\int_{-\infty}^{\infty} |\Psi_{||}(z, t)|^2 dz], \quad (24)$$

where

$$V_\perp = \frac{m \omega_\perp^2 |\vec{r}_\perp|^2}{2} - \alpha(\omega) \epsilon_0 |E(\vec{r}_\perp)|^2 \quad (25)$$

Because of normalization

$$\int_{-\infty}^{\infty} |\Psi_{||}(z, t)|^4 dz = 1/2 \quad \text{and} \quad \int_{-\infty}^{\infty} |\Psi_{||}(z, t)|^2 dz = 1 \quad (26)$$

and the following 2D GPE results from separation of variables for "pancake" trap:

$$i\hbar \frac{\partial \Psi_{\perp}}{\partial t} = -\frac{\hbar^2}{2m} \Delta_{\perp} \Psi_{\perp} + V_{\perp}(r_{\perp}^{\rightarrow}) \Psi_{\perp} + \frac{4\pi\hbar^2 a(\vec{B})}{m} \Psi_{\perp} |\Psi_{\perp}|^2 \quad (27)$$

The scattering length a as a function of magnetic field is:

$$a(\vec{B}) = a_{bg} \left(1 + \frac{\Delta_B}{B - B_{peak}} \right) \quad (28)$$

where Δ_B is a width of Feshbach resonance, B_{peak} - resonant magnetic field, a_{bg} -background scattering length[2].

Formally the separation of variables is applicable each time when Hamiltonian is a sum of components depending on different groups of variables, but this method have additional physical meaning for asymmetric potentials, like elongated in z -direction trap [14] or "pancake" 2D trap (fig. 1) as in current case. The dynamics of Ψ in 2D traps was considered in large amount of papers, including the geometries of periodic potentials, Bessel lattices etc. In current case the SFV lattice under consideration has some peculiarities, qualitatively described above in discussion of classical motion of dipole around phase singularity.

Let us try to seek the simplest solution of equation (27) which describe the main feature of optical vortex array as a trapping field, namely the continuous transfer of angular momentum from OV to BEC wavefunction Ψ . Because the direction of rotation of classical particle is determined by distribution of TC of OV ℓ_{EM} of trapping beam the distribution of TC's in quantum SFV lattice l_{BEC} will be set identical to those of trapping field.

We will seek for solution of this equation presuming the identical spatial distributions for fields $\Psi_{\perp}(r_{\perp}^{\rightarrow}, t)$ and $E(r_{\perp}^{\rightarrow})$. It means that Ψ is also a sum of a GL functions with alternating topological charges ℓ_{EM} (see eq.(16)). The effective diameter of the core b is assumed to be equal to effective size of GL beam bottleneck (4-10 μm).

Formally correlation K of two complex spatially inhomogeneous fields $\Psi_{\perp}(r_{\perp}^{\rightarrow}, t)$ and $E(r_{\perp}^{\rightarrow})$ must be equal to unit:

$$K = \frac{|\int \Psi_{\perp} E^*(r_{\perp}^{\rightarrow}) d^2 r_{\perp}^{\rightarrow}|^2}{[\int |\Psi_{\perp}|^2 d^2 r_{\perp}^{\rightarrow}][\int |E(r_{\perp}^{\rightarrow})|^2 d^2 r_{\perp}^{\rightarrow}]} = 1 \quad (29)$$

The key point is in adjusting the parameters in $\Psi_{\perp}(r_{\perp}^{\rightarrow}, t)$ and $E(r_{\perp}^{\rightarrow})$ in such a way that two last terms in (24) would cancel each other. This might happen when following condition is imposed on coefficients:

$$\alpha(\omega) \epsilon_0 |E_0|^2 = \frac{2\pi\hbar^2 a(\vec{B})}{m} \quad (30)$$

Consider first the case of single vortex trap collocated with a single parabolic subtrap:

$$V_{\perp} = \frac{m\omega_{\perp}^2 r^2}{2} - \alpha(\omega) \epsilon_0 |E_0|^2 r^2 \exp[-r^2/d^2] \quad (31)$$

Separation of variables in potential for longitudinal and transverse component results in the following wavefunction familiar with already mentioned variational solution (11) [24]:

$$\Psi_{\perp} = \sqrt{\frac{2}{\pi}} \left[\frac{m\omega_{\perp}}{\hbar} \right]^{3/2} r \exp \left[-\frac{m\omega_{\perp}^2 r^2}{2\hbar} + i\phi \ell_{BEC} - i2\omega_{\perp} t \right] \quad (32)$$

Note this is exact wavefunction of the transversal GPE, in contrast to variational solution (11). The stability analysis will be published elsewhere. The angular momentum per particle is given by:

$$\langle \hat{\ell} \rangle = \int \int \Psi_{\perp}^* (-i\hbar) \frac{\partial \Psi_{\perp}}{\partial \phi} d^2 r_{\perp}^{\rightarrow} = \hbar \quad (33)$$

where ϕ is azimuthal angle. Again SFV carries angular momentum \hbar per particle and kinetic energy per unit length of the vortex line $E_{kin} = N\pi\hbar^2 \chi \ln(\tilde{b}/\tilde{a})/m$, where \tilde{b} -diameter of vortex core, \tilde{a} -interatomic distance [16].

Consider now the trapping of BEC by of phase-locked Gaussian-Laquerre beams placed at the nodes i, j of rectangular grid of period p (see Eq. 8).

Let us assume that optical wavelength λ is equal to De-Broigle wavelength λ_{db} :

$$\lambda = \lambda_{db} = \frac{\hbar}{\sqrt{2mk_B T}} \quad (34)$$

The corresponding BEC temperature for ^{85}Rb atoms is:

$$T = 1.7^{-7} K \quad (35)$$

After imposing compensation condition (26) the residual part of transverse GPE (27) corresponds to free-space evolution:

$$i\hbar \frac{\partial \Psi_{\perp}}{\partial t} = -\frac{\hbar^2}{2m} \Delta_{\perp} \Psi_{\perp} + \frac{m \omega_{\perp}^2 r^2}{2} \Psi_{\perp} \quad (36)$$

The free space propagation (fig. 1) equation for EM-field will be of similar form:

$$\frac{\partial E}{\partial z} = -\frac{i}{2k} \Delta_{\perp} E + \frac{k r^2}{2f_{cavity}} E \quad (37)$$

where f_{cavity} is effective focal length of the laser cavity (fig. 1) induced by thermal lensing of inhomogeneity of optical pumping. Because of linearity of equation and superposition principle the solution will be the sum of Gaussian wave packets including zero-order Gaussian functions, Gaussian-Hermit or Gaussian-Laguerre modes located at sites $\vec{r}_{jx,jy}$ [11] separated by period p . The axes of array are parallel to X, Y . The numerical modeling of eq. (27) via split-step FFT method [21] had been performed. The mesh size jx, jy in plane was $512 \cdot 512$ points, the "guard bands ratio" [25] was chosen equal to 8. So the main part of the field Ψ was located inside central part of a mesh of $64 \cdot 64$ size - the "image area". The tolerance of the energy spillover was kept within $\epsilon_1 = 0.0001$. The windowing in wavenumber space after FFT at each timestep was performed by usage of "Fermi-Dirac" smoothed step function [21]. The dissipation inherent to split-step FFT method have led to decrease of total "amount of particles" $\int \int |\Psi|^2 dx dy$ within "image area" at a speed of 10^{-3} per time step. The special initial conditions of "preselected" SFV array in the form (8) superimposed upon homogeneous background gave the spatial distribution of "transverse" wavefunction Ψ_{\perp} well correlated ($K = 0.7$) with the OVA array distribution - the array of phase-locked Gaussian-Laguerre wavepackets of the first order :

$$\Psi_{\perp} = \frac{2}{\pi} \left[\frac{m\omega_{\perp}}{\hbar} \right]^{3/2} \sum_{jx,jy} (|\vec{r} - \vec{r}_{jx,jy}|) \exp(-|\vec{r}|^2/D^2) \exp\left[-\frac{m\omega_{\perp}^2 |\vec{r} - \vec{r}_{jx,jy}|^2}{2\hbar}\right] + \\ i \ell_{BEC} \text{Arg}(\vec{r} - \vec{r}_{jx,jy}) + i \pi(jx + jy) - i 2 \omega_{\perp} t \quad (38)$$

The interesting feature of this solution $\Psi = \Psi_{\perp} \Psi_{\parallel}$ of GPE is that it is very close to the linear combination of Gaussian-Laguerre functions. Nevertheless the interference between wavefunctions of "subvortices" is taken into account, because the "doughnut" radius is set to be a bit less than distance between lattice nodes. The arising interference pattern is well correlated with the interference pattern produced by Gaussian-Laguerre OV array $|E(\vec{r}_{\perp})|^2$ (fig. 3) with the same geometrical parameters and wavelength λ . Evidently the stability of such "linear" solution of nonlinear equation is essential and it will be published elsewhere.

Each SFV carries angular momentum \hbar per particle and rotational kinetic energy $E_{kin} = N\pi\hbar^2 \chi \ln(\tilde{b}/\tilde{a})/m$, \tilde{b} - diameter of vortex core, \tilde{a} - interatomic distance, χ - length of vortex which is roughly equal to thickness of "pancake" [16]. In contrast to superfluid in rotating bucket where angular momenta of vortices are co-directed [15], the BEC vortices trapped by optical vortex array are counter-directed from site to site. Thus in the net sum of angular momenta each vortex of positive topological charge is compensated by the term with negative charge and total angular momentum tends to zero. Nevertheless the mutual subtraction of angular momenta (vectorial) of adjacent vortices in the net sum does not mean the mutual subtraction of rotational energies, which are the positive scalars. The ground state carry substantial amount of rotational kinetic energy of condensate containing N particles of mass m per unite volume, namely $E_{rot} = N_{vortices} N \pi \hbar^2 \chi \ln(\tilde{b}/\tilde{a})/m$.

VI. CONCLUSION

The optical vortex arrays emitted by solid-state microchip laser are analysed from the point of view of application to optical dipole traps. The possible equivalent being highly correlated to numerically obtained and experimentally observed EM-field distributions proved to be an array of Gaussian-Laguerre beams equispaced at the nodes of rectangular lattice. For macroscopic wavefunction Ψ of BEC trapped in such complex optical field the analytical solutions of Gross-Pitaevsky equation were found based on separation of variables and mutual compensation of vortex component of external trapping field via nonlinear term of GPE. The obtained wavefunctions have perfect correlation with trapping field, including distribution of topological charges, which form antiferromagnetic-like lattice. Within framework of this particular model the "antiferromagnetic" lattice of BEC vortices carries total angular momentum close to zero while net rotational kinetic energy of SFV lattice tends to be equal to the sum of rotational energies of vortices. The field of classical velocities obtained via Madelung transform, i.e. the field of phase gradient forms labyrinth structure. In classical picture the trapped particle moves across the vortex array labyrinth jumping from one whirl to another.

In quantum picture represented via analytic solution of GPE the coherent macroscopic wavefunction extends all over OV trapping array with transverse spatial dimension of several hundred microns. The complex field of velocities, substantial rotational energy and high degree of correlation of SFV wavefunction with OV trapping field promise more resistance to decoherence.

The qualitative analytic solution supports the basic feature related to trapping of transparent particles and to BEC trapping: the transfer of OAM from EM-field to superfluid. The proposed OVA trap might be interesting from the point of view of studies of quantum-classical correspondence.

In quantum computing the mechanism of imposing the topological charges to BEC vortices by means of manipulating the vorticity of trapping optical array could result in demonstration of macroscopic quantum interference phenomena. Evidently there are 4 possible topologically equivalent combinations of parameters of solution (38) of OV charges ($\ell_{EM} = \pm 1$) and their relative phases ($\pm \pi$). Thus there exist 4 wavefunctions Ψ having the identical probability $|\Psi|^2$ distribution and different orientation of SFL vortices with respect to physical axes X, Y of trapping setup, characterised by ℓ_{BEC} and their relative phases. The transformation of the one Ψ into another one having different phase structure is equivalent to 90° rotation around z - axis.

-
- [1] R.Grimm, M.Weidemuller and Yu.B.Ovchinnikov., "Optical dipole traps for neutral atoms" *Adv.At.Mol.Opt.Phys.* **42**, 95 (2000).
 - [2] L. Pitaevskii and S. Stringari., "Bose-Einstein Condensation", Clarendon Press, Oxford, 2003.
F. Dalfovo, S.Giorgini, S.Stringari, L.P.Pitaevskii., "Theory of Bose-Einstein condensation in trapped gases", *Rev.Mod.Phys.* **71**, 463 (1999).
 - [3] Balykin, V.I., Letokhov, V.S., Ovchinnikov, Yu.B., and Sidorov A.I., "Quantum-State-Selective Mirror Reflection of Atoms by Laser Light", *Phys. Rev. Lett.* **60**, 2137 (1988),
 - [4] E. M. Wright, J. Arlt and K. Dholakia., "Toroidal Optical Dipole Traps for Atomic Bose-Einstein Condensates using Laguerre-Gaussian Beams", *Phys.Rev. A* **63**, 013608 (2001).
 - [5] A.Yu.Okulov., "3D-configuration of the vortex lattices in microchip laser cavity",
QCMC-2004, AIP Conference Proceedings, **734**, p.366 (2004).
A.Yu.Okulov., "3D structure of the vortex lattices in solid-state microchip laser", *Bulletin Lebedev Physical Institute*, **9**, p.3, Sept. (2003).
 - [6] Yu.B.Ovchinnikov., "Coherent manipulation of atoms by copropagating laser beams ", *Phys.Rev.*, **73A**, 033404 (2006).
 - [7] R.Dumke, M.Volk, T. Muther, F.B.J.Buchkremer, G. Birkl and W.Ertmer., "Microoptical Realization of Arrays of Selectively Addressable Dipole Traps: A Scalable Configuration for Quantum Computation with Atomic Qubits ", *Phys. Rev. Lett.* **89**, 097903 (2002).
 - [8] M. Babiker, W. L. Power, and L. Allen., "Light induced torque on moving atom", *Phys. Rev. Lett.* **73**, 1239 (1994).
 - [9] V.Garces-Chavez, D. McGloin, M. J. Padgett, W. Dultz, H. Schmitzer, and K. Dholakia., "Observation of the Transfer of the Local Angular Momentum Density of a Multiringed Light Beam to an Optically Trapped Particle", *Phys. Rev. Lett.* **91**, 093602 (2003).
 - [10] M.J.Frieze, J.Euger, H.Rubinstein-Dunlop., " ", *Phys.Rev. A* **54**, 1543 (1996).
N.R. Heckenberg, M.E.J. Frieze, T.A. Nieminen and H. Rubinsztein-Dunlop., "Mechanical Effects of Optical Vortices". pp 75-105, in M. Vasnetsov (ed), *Optical Vortices*, Nova Science Publishers (1999).
 - [11] A.Yu.Okulov., "Two-dimensional periodic structures in nonlinear resonator", *JOSA* **B7**, p.1045, (1990).
 - [12] J.Courtial, R.Zambrini, M.R.Dennis, M.Vasnetsov., "Angular momentum of optical vortex arrays ", *Optics Express* **14**, p.938 (2006).
 - [13] Y.F.Chen, Y.P.Lan., "Formation of optical vortex lattices in solid-state microchip lasers: Spontaneous transverse mode locking ", *Phys.Rev.*, **64A**, 063807 (2001),

- Y. F. Chen, Y. P. Lan., "Transverse pattern formation of optical vortices in a microchip laser with a large Fresnel number", *Phys. Rev.*, **65**, 013802 (2001).
- [14] R. Fidele, P. K. Shukla, S. De Nicola, M. A. Manko, V. I. Manko, F. S. Cataliotti. "Controlling potential traps for filtering solitons in Bose-Einstein condensates", *JETP Lett.*, **80**, 8, p.609-613 (2004).
- [15] J. R. Abo-Shaerr, C. Raman, J. M. Vogels and W. Ketterle., "Formation and Decay of Vortex Lattices in Bose-Einstein Condensates at Finite Temperatures", *Phys. Rev. Lett.* **88**, 070409 (2002).
- [16] R. P. Feynman, "Statistical mechanics", Ch. 11, Reading, Massachusetts (1972).
- [17] A. Yu. Kitaev., LANL e-print quant-ph/ 9707021, <http://arxiv.org>, (1997).
- [18] K. Staliunas., "Laser Ginzburg-Landau equation and laser hydrodynamics", *Phys. Rev. A* **48**, 1573 (1993). K. Staliunas, C. O. Weiss., "Nonstationary vortex lattices in large-aperture class B lasers", *JOSA B* **12**, 1142 (1995).
- [19] F. Hollinger, Chr. Jung, and H. Weber., "Simple mathematical model describing multitransversal solid-state laser", *JOSA B* **7**, 1013 (1990).
- [20] A. E. Siegman., "Lasers". *University Science Books, Mill Valley, California* (1986).
- [21] A. Yu. Okulov., "Scaling of diode-pumped solid-state lasers via self-imaging", *Opt. Comm.*, **99**, p.350-354 (1993)., "The effect of roughness of mirrors on transverse structure of light field in nonlinear Talbot cavity", *J. Mod. Opt.*, **38**, N.10, p.1887 (1991).
- [22] A. Yu. Okulov., "Gain-mode correlation in diode-pumped solid-state laser", *Optics and Spectroscopy.*, **77**, N6, p.985 (1994).
- [23] V. Garces-Chavez, K. Volke-Sepulveda, S. Chavez-Cerda, W. Sibbett and K. Dholakia., "Transfer of orbital angular momentum to an optically trapped low-index particle", *Phys. Rev. A* **66**, 063402 (2002).
- [24] J. Tempere and J. T. Devreese, E. R. I. Abraham., "Vortices in Bose-Einstein condensates confined in a multiply connected Laguerre-Gaussian optical trap", *Phys. Rev.*, **64A**, 023603 (2002).
- [25] E. A. Sziklas, A. E. Siegman., "Mode calculations in unstable resonators with flowing saturable gain. 2: Fast Fourier transform method", *Appl. Opt.*, **14**, 1874 (1975).

List of Figure Captions

Fig.1. Conceptual view of the near field optical trap. Upper plot: Transverse (in XOY plane) distribution of intensity in the near field of solid-state microchip laser [5]. Middle: The longitudinal scale extends to 6 Talbot lengths. Z - axis is directed along optical axis of microchip laser resonator(bottom) . Additional tightly confined parabolic well keeping BEC cloud localized in z - direction is depicted via potential $V(z) \approx (z - z_0)^2$. Such potential is assumed to be superimposed by the other microchip laser beam with cylindrical focusing lens at slightly different wavelength of radiation from the range $0.98 \div 2.79 \mu m$, in order to avoid interference. Fresnel number has value of $N_f \approx N_{vortices}^2 = 64$.

Fig.2.Diffractive self-imaging of two-dimensional lattice of 8x8 Gaussian beams with period $p = 28 \mu m$. The longitudinal cross-section at $y = 0$ plane of intensity distribution $I(x, y, z)$ presented. The lattice is self-reproduced at Talbot distance, spatial period division occurs at quarter Talbot distances and central lobe forms outside the Rayleigh range.

Fig.3.Intensity distribution in transverse plane of artificial Gaussian-Laquerre vortex array. Vortices(dark holes) are at nodes of rectangular grid. Letters ℓ_{EM} denote vortices with alternating topological charge, changing sign from one site of lattice to another.

Fig.4.Longitudinal section of vortex array in the near field in x - z plane at $y = 0$ section. The vortex lines are parallel, the topological charges ℓ_{EM} are flipping from one vortex line to another. The wavelength $\lambda = 1 \mu m$, period p of lattice both in x and y directions is $30 \mu m$.

Fig.5.Helicoidal phase surface of Gaussian-Laquerre beam. Atomic dipole having "red" detuning moves along phase gradient. Trajectory is located at maximum of intensity. \vec{S}_t is the component of Pointing vector tangent to helix. The major component of \vec{S}_z is directed parallel to beam propagation, i.e. along Z-axis.

Fig.6.Helicoidal phase surface of Gaussian-Laquerre beam array. The elementary cell consists of four vortices. The adjacent vortices have alternating topological charges ℓ_{EM} and alternating angular momenta . In classical picture the atomic dipole moves along phase gradient of a given vortex next it jumps to another one.

Fig.7.The argument of macroscopic wavefunction Ψ , corresponding field of velocities, obtained via Madelung transform and distribution of modulus of wavefunction. The superfluid vortices form the lattice with alternating topological charges $\ell_{BEC} = \pm 1$. The elementary cell consists of four BEC vortices whose locations are identical to the vortices of trapping EM-field. Horizontal pair has the same charges ℓ_{BEC} which are π -shifted with respect to each other, the vertical pair have π -shifted $-\ell_{BEC}$ charges. The adjacent vortices have alternating topological charges and alternating angular momenta \hat{L} in contrast to superfluid in rotating bucket which forms the lattice with co-directed angular momenta. The alternating charges ℓ_{BEC} makes the field of velocities continuous. The square modulus of Ψ is shown at the right insert.

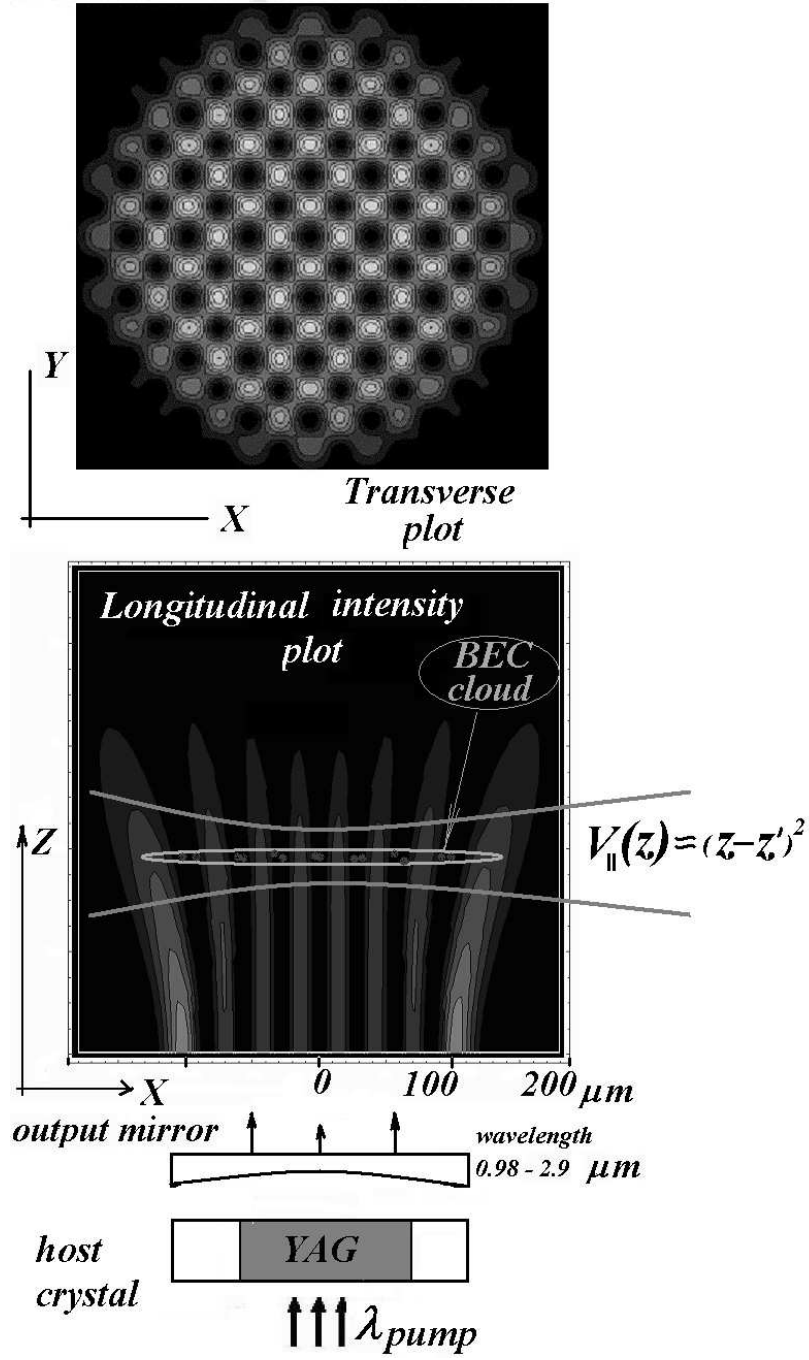


FIG. 1: Conceptual view of the near field optical trap. Upper plot: Transverse (in XOY plane) distribution of intensity in the near field of solid-state microchip laser [5]. Middle: The longitudinal scale extends to 6 Talbot lengths. Z - axis is directed along optical axis of microchip laser resonator(bottom) . Additional tightly confined parabolic well keeping BEC cloud localized in z - direction is depicted via potential $V(z) \approx (z - z_0)^2$. Such potential is assumed to be superimposed by the other microchip laser beam with cylindrical focusing lens at slightly different wavelength of radiation from the range $0.98 \div 2.79 \mu m$, in order to avoid interference. Fresnel number has value of $N_f \approx N_{vortices}^2 = 64$.

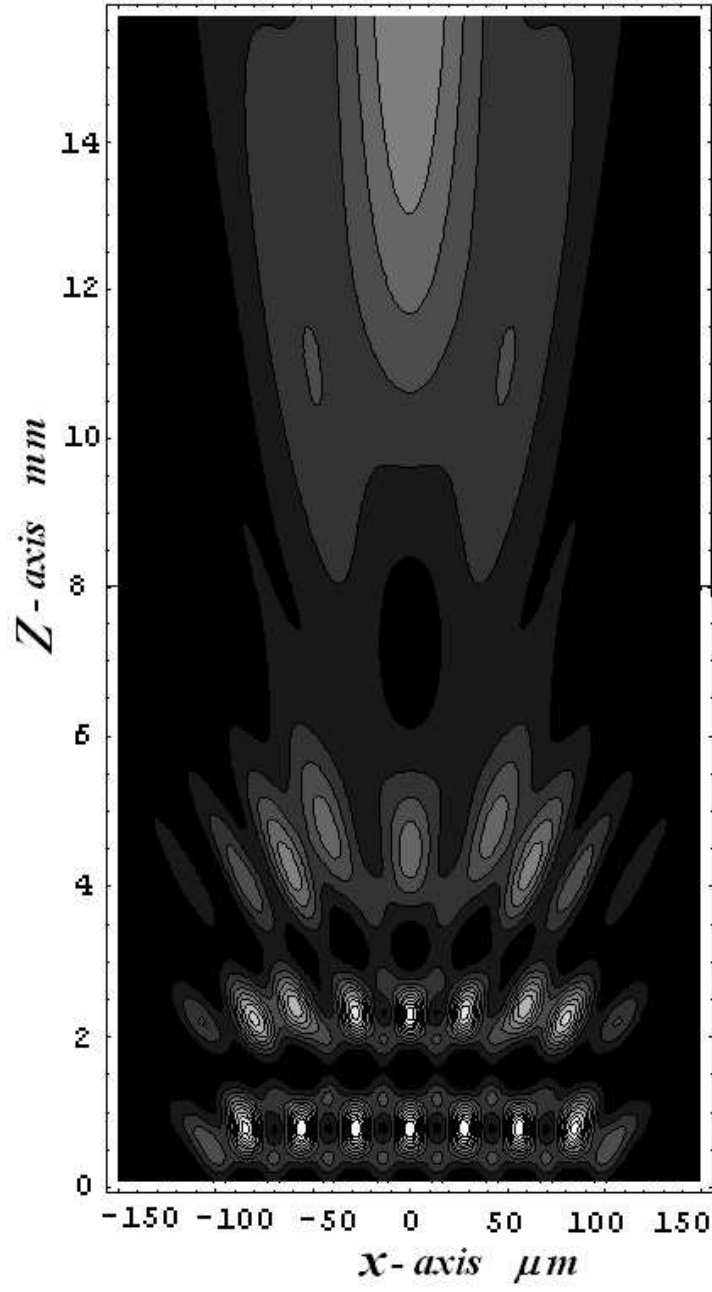


FIG. 2: Diffractive self-imaging of two-dimensional lattice of 8×8 Gaussian beams with period $p = 28 \mu m$. The longitudinal cross-section at $y = 0$ plane of intensity distribution $I(x, y, z)$ presented. The lattice is self-reproduced at Talbot distance, spatial period division occurs at quarter Talbot distances and central lobe forms outside the Rayleigh range.

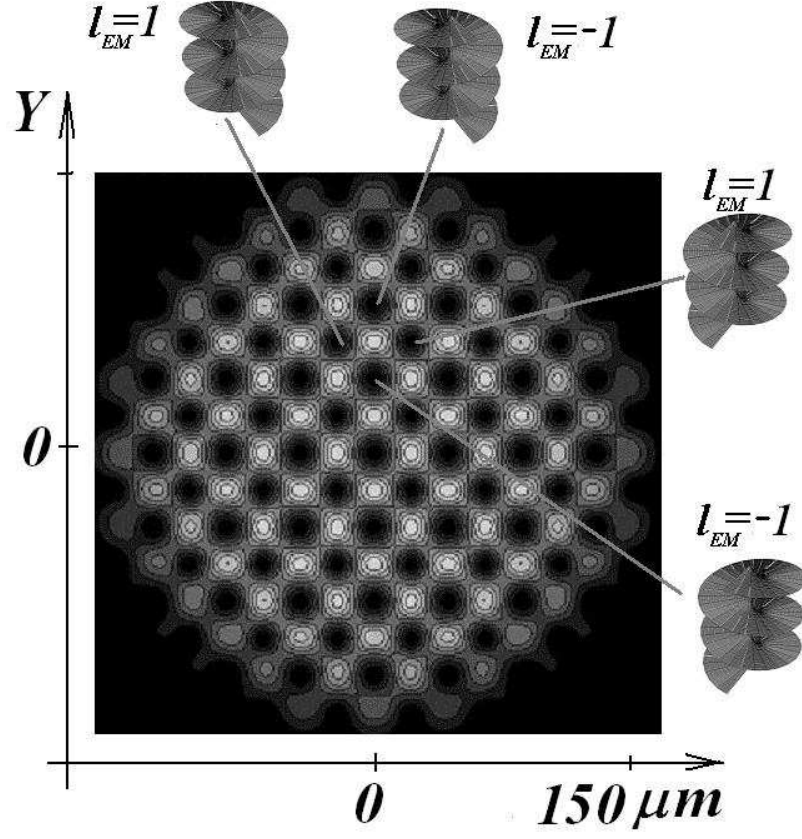


FIG. 3: Intensity distribution in transverse plane of artificial Gaussian-Laguerre vortex array. Vortices (dark holes) are at nodes of rectangular grid. Letters l_{EM} denote vortices with alternating topological charge, changing sign from one site of lattice to another.

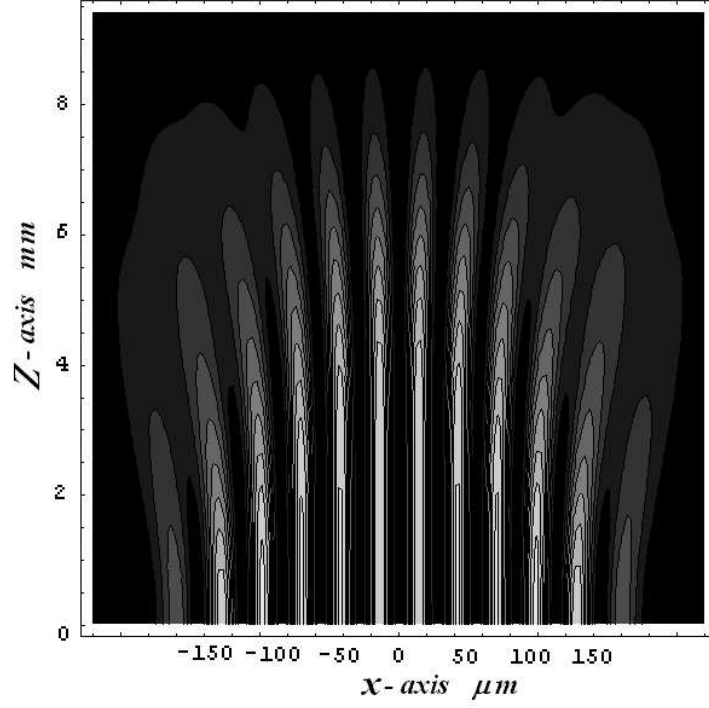


FIG. 4: Longitudinal section of vortex array in the near field in x - z plane at $y = 0$ section. The vortex lines are parallel, the topological charges ℓ_{EM} are flipping from one vortex line to another. The wavelength $\lambda = 1\mu m$, period p of lattice both in x and y directions is $30\mu m$

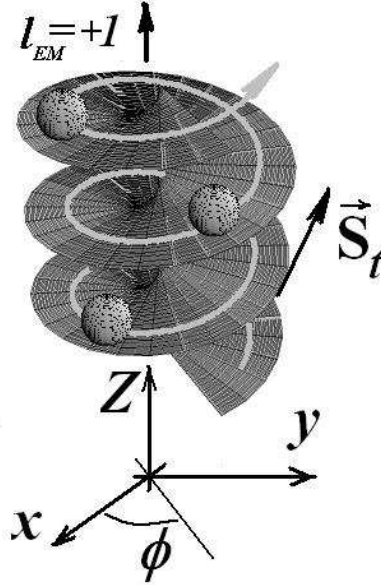


FIG. 5: Helicoidal phase surface of Gaussian-Laguerre beam. Atomic dipole having "red" detuning moves along phase gradient. Trajectory is located at maximum of intensity. \vec{S}_t is the component of Poynting vector tangent to helix. The major component of \vec{S}_z is directed parallel to beam propagation, i.e. along Z -axis.

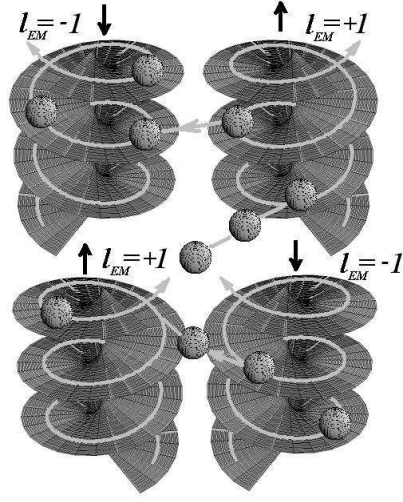


FIG. 6: Helicoidal phase surface of Gaussian-Laguerre beam array. The elementary cell consists of four vortices. The adjacent vortices have alternating topological charges ℓ_{EM} and alternating angular momenta. In classical picture the atomic dipole moves along phase gradient of a given vortex next it jumps to another one.

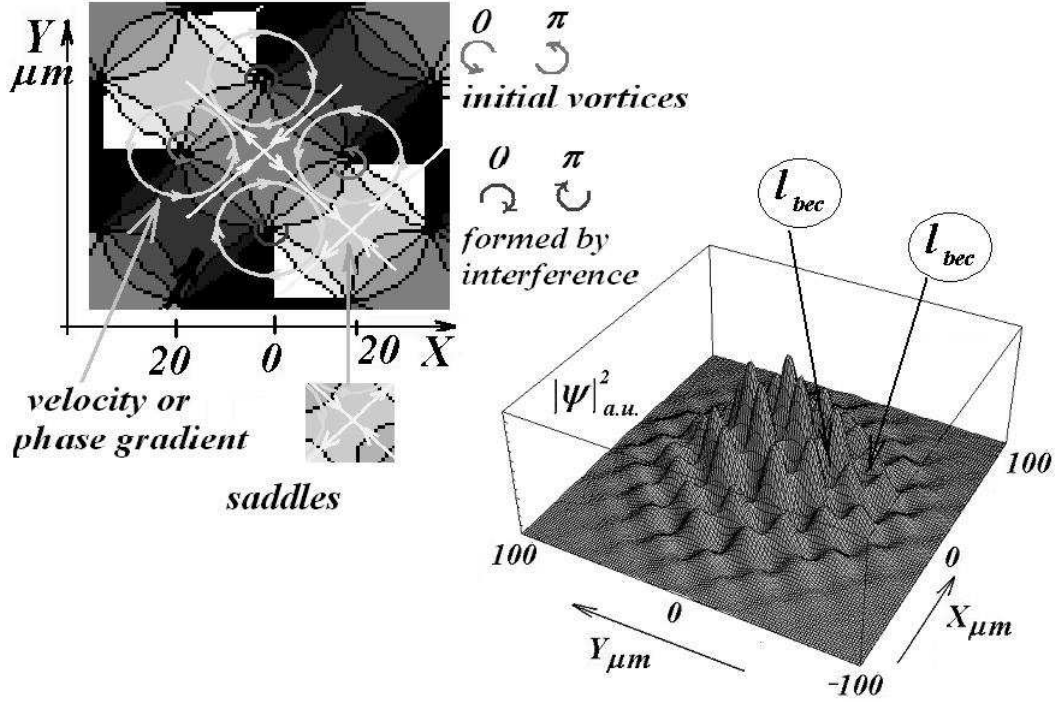


FIG. 7: The argument of macroscopic wavefunction Ψ , corresponding field of velocities, obtained via Madelung transform and distribution of modulus of wavefunction. The superfluid vortices form the lattice with alternating topological charges $\ell_{BEC} = \pm 1$. The elementary cell consists of four BEC vortices whose locations are identical to the vortices of trapping EM-field. Horizontal pair has the same charges l which are π -shifted with respect to each other, the vertical pair have π -shifted $-\ell_{BEC}$ charges. The adjacent vortices have alternating topological charges and alternating angular momenta \hat{L} in contrast to superfluid in rotating bucket which forms the lattice with co-directed angular momenta. The alternating charges ℓ_{BEC} makes the field of velocities continuous. The square modulus of Ψ is shown at the right insert.